dislocation annihilation increases in the longer time of BM while dislocation cells continue to decrease, and gradually reaches an equilibrium with dislocation propagation so that the domain size slowly decreases [40]. The fact that the shape, size and preferred orientation as well as the density of lattice defects such as grain boundaries, dislocations, etc. do not change is generally known as an index of the stable dynamic state during BM.

In Fig. 4, only Al peaks could be observed. No Al_2O_3 peaks were detected, which can be explained by the very low quantality of Al_2O_3 and the limited detectability of the XRD device. The relative intensity of the Al peaks has obviously altered, confirming that the statistically preferred orientation in as-milled Al flakes after cold welding. Therefore, it can be concluded that cold welding destroys the regularity of the as-milled Al flakes, which was also confirmed by the XRD patterns of the cold-welded powder.

The BM process transforms the initial Al powder into flaky particles with a preferred orientation through a combination of deformation, cold welding and fragmentation [41,42]. As milling progresses, the hardness of the particles increases, reducing their malleability and increasing the likelihood of fracture upon further deformation [43]. Ultimately, the morphology of the particles stabilizes as a balance between fracture and cold welding is achieved. With this process, the microstructural properties of the Al powder, including the size, texture and thickness of the flakes, can be effectively tunned.

3.1. *Microstructures of sintered and extruded Al/Al_2O_3 composite with different cold welding times*

The change in the morphology of the Al powders leads to different architectures of the Al/Al_2O_3 composite. The SEM images of the fracture surface in the Al/Al_2O_3 composite after 15 min, 1 h and 2 h cold-welding are shown in Fig. 5. The change in the morphology of the Al powders leads to different architectures of the Al/Al_2O_3 composite. The SEM images of the fracture surface of the Al/Al_2O_3 composite after 15 min, 1 h and 2 h cold welding are shown in Fig. 5. The fracture surface of the 15 min cold-welded specimen in Fig. 5(a) shows a well-preserved laminate characterized by the parallel cracks. While the cold-welded 1 h specimen in Fig. 5(b) shows a combined morphology of lamellar and equiaxed grains. As can be seen from Fig. 5(b), the short cold welding resulted in a partial disruption of the laminated microstructure and the Al_2O_3 platelets in the less well-organized regions were incorporated both at the grain boundaries and in the grain interior of the Al. Both samples showed typical ductile fracture surfaces consisting of fine and almost homogenous dimples. This indicates that no obvious localized early failure occurred in the specimens that were cold welded for 1 h or even 15 min. The fracture surface of the cold-welded 2 h specimen in Fig. 5(c) shows no laminate features, only equiaxed grains. It can be seen that the dimples in the 2 h cold weld aligned upwards and coalesced in the tensile direction, whereas the dimples in the 15 min cold weld extended parallel to the tensile direction. This type of fracture provides significant evidence of the strong lateral constraint created by Al_2O_3 at the Al grain boundaries during the phase of high plastic strain.

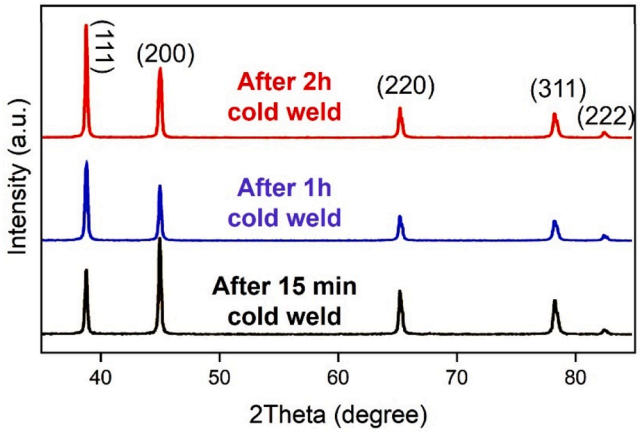

Fig. 4. XRD patterns of the cold-welded powders with different milling time.

It is clear that cold welding has destroyed the laminated microstructure, which is also confirmed by the TEM images. Fig. 6(a-c) shows the microstructures of the Al/Al_2O_3 composite after 15 min, 1 h and 2 h cold welding.

The 1 h cold-welded sample in Fig. 6(b) shows a mixed microstructure with HAGBs decorated by Al_2O_3 nanoplatelets (Fig. 6(b)). Short-term cold welding only partially destroyed the laminated microstructure and the Al_2O_3 nanoplatelets in the disordered areas were inserted into the grain interior. The non-destroyed areas remained the same in the 15 min cold welding sample and the distance between the layers of the non-destroyed areas became slightly finer. The 2 h cold-welded sample in Fig. 6(c) shows a completely disordered microstructure with Al_2O_3 nanoplatelets randomly distributed in the equiaxed grains.

The laminated feature of the 15 min cold weld sample maintained well and Al_2O_3 nanoplatelets lies on the lamellar grain boundaries as proved by EDS oxygen mapping in Fig. 7 (a-c). MThe laminated feature of the 15-min cold sweat sample was well preserved and the Al_2O_3 nanoplatelets are located at the lamellar grain boundaries, as shown by the EDS oxygen mapping in Fig. 7 (a-c). Most of the Al_2O_3 nanoplatelets are obviously located in both the HAGBs and the grains and are arranged in a line, as shown in Fig. 7 (d, f). The formation of γ-Al_2O_3 on Al-GBs or triple junctions because of thermodynamic considerations related to energy [44–46]. Since the highest processing temperature and annealing treatment in this study is higher than 450 ℃ [47], the transformation of amorphous Al_2O_3 → γ-Al_2O_3 is expected to occur as a temperature-dependent transformation [47,48] (Fig. 7(e)). Previous work on forged, extruded and sintered Al powders sintered at up to 600 °C clearly confirmed a γ-Al_2O_3 phase derived from the amorphous precursor and exhibiting a cubic lattice structure (fcc structure, (Fd-3 m) space group, lattice parameter 0.7677 ± 0.005 nm) [14,47,49-51]. As the intensity of the BM process increases with increasing speed, more Al_2O_3 nanoplatelets are generated, which detach from the previous powder surface and redistribute on the HAGBs and in the grain interior. It can be inferred that as long as the Al_2O_3 dispersoid is positioned in the γ-Al_2O_3 form with a preferential orientation at the HAGBs, its influence is strong [52]. In other words, with increasing energy input to the powders, the transformation of amorphous Al_2O_3 → γ-Al_2O_3 is gradually facilitated (due to the increase of vital temperature caused by intense collisions and friction) and converted into γ-Al_2O_3 particles, which strongly affects the Zener pressure opposing the motion of GB. Therefore, it is more likely that the pinning effect on the GBs becomes weaker as the Al_2O_3 particles increase. Obviously, the 15 min cold-welded sample retained the laminated structure after extrusion. The distance between the lamellae did not change significantly. The 2 h cold weld does not show clear laminate boundaries. The samples cold-welded at 15 min and 1 h show no obvious microstructural changes, but a strong alignment of the Al_2O_3 nanoplatelets

The mean grain sizes of the samples were counted using TEM images considering average of 300 grains (Fig. 6d). The results are 480 nm, 450 nm and 340 nm for the 15 min cold weld,1 h cold weld and 2 h cold weld samples respectively. The mean grain sizes of the samples were counted using TEM images taking an average of 300 grains (Fig. 6d). The results are 480 nm, 450 nm and 340 nm for the 15 min cold welded, 1 h cold welded and 2 h cold welded samples respectively. It is known that as the milling process progresses, lamellar particles are formed as a result of cold welding of the flattened particles. At the same time, Al_2O_3 nanoplatelets, which adhere to the surface of the aluminum particles, are trapped between the lamellar gaps. Accordingly, the grain shape of the composite grains shifts from a lamellar to an equiaxed morphology. It is worth noting that the lamellar boundaries for the competition between cold welding and fracture are distorted and a random weld orientation is

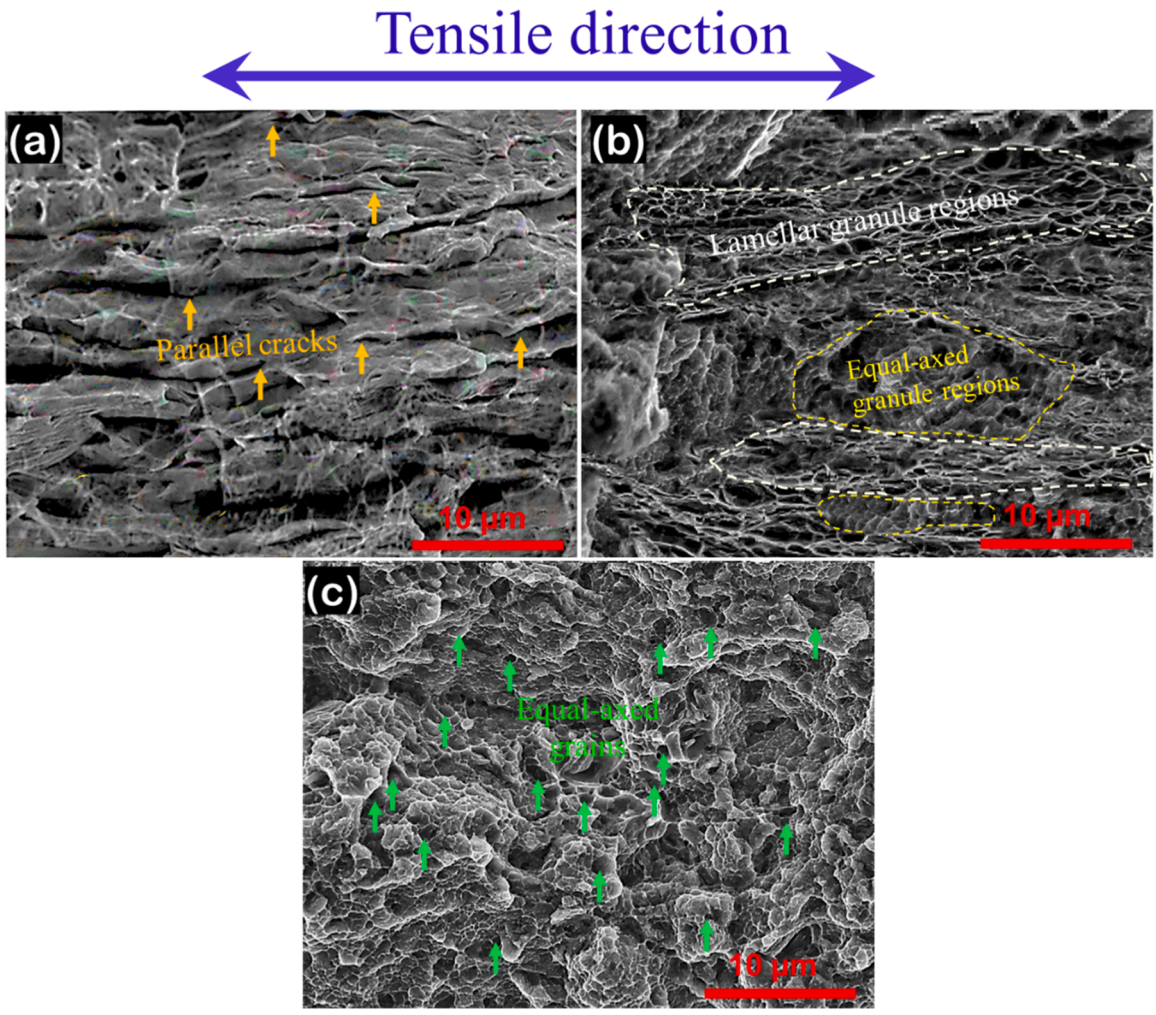

Fig. 5. Tensile fracture morphology of (a)15 min cold-weld, (b) 1 h cold weld and (c) 2 h cold weld, of the sintered compacts. The orange and green arrows indicate parallel fractures and grains with equal-axed grains, respectively. Dashed white and yellow lines also depict areas of lamellar and equal-axed grain structures, respectively. The fractures are aligned parallel to the tensile direction.

formed. Cold welding had a strong influence on grain refinement, which can increase the mechanical strength of the final Al/Al_2O_3 composite. Details are discussed in the next section.

Fig. 8 is the typical XRD pattern in cross-section of the extruded samples.

For the three samples processed under different BM conditions, the Schmid factor has almost the same values (Fig. 1S), indicating that the proportion of texture reinforcement is almost the same for all three samples. These slight differences in the Schmid factor values are probably due to the particular arrangement of the Al_2O_3 nanoplatelets in agreement with Jiang et al. [53]. Such Schmid factor values (which are almost very high compared to other Al composites [54,55]) must logically represent a high degree of slip. However, the 1 h cold-welded sample shows the best combination of strength and ductility compared to the other samples indicating that the Al_2O_3 in the HAGBs prevents grain rotation or sliding of the grain boundaries during extrusion. Thus, converting the laminated architecture to an equiaxed architecture by increasing the cold-welding time from 15 min to 2 h leads to Al_2O_3 detachment on the HAGBs, resulting in grain rotation, grain boundary sliding, and subsequent dynamic recrystallization.

In general, with increasing duration of cold welding, the laminated microstructure gradually disappeared and the lamellar grains transformed into equiaxed grains. Extrusion merely refined the microstructures without destroying the microstructure of the sintered sample. Together with the transformation of the grains, the in-situ formed Al2O3 also changed location from the lamellar grain boundaries to the grain interior during cold welding. Cold welding thus effectively and significantly changed the architecture, i.e. the grain shapes and the location of the Al_2O_3, of the Al/ Al_2O_3 composites. Samples with different cold-welding times represent different types of architectures: laminated features for the 15 min cold-welding sample, random features for the 2 h cold-welding sample and mixed features for the 1 h cold-welding sample.

4. Mechanical properties of the Al/Al_2O_3 composites with different architectures

The tensile stress-strain curves of the extruded Al/Al_2O_3 composites with different architectures are shown in Fig. 9(a). Detailed data are listed in Table 1.

The 2 h cold-welded sample has the highest tensile strength (UTS) of 390 MPa and the lowest ductility of only 6.7 %, while the 15 min cold-welded sample has a relatively lower UTS of 356 MPa but more than twice the ductility of 13.3 %. The 1 h cold welded sample shows a mediocre mechanical performance between the 15 min cold welded and the 2 h cold welded sample. Classical analytical models were used to find out the underlying strengthening and toughening mechanisms of Al/Al_2O_3 composites in the initial state with different architectures.

The 0.2 % yield strength of the Al/Al_2O_3 composites fabricated in this study can be expressed as:

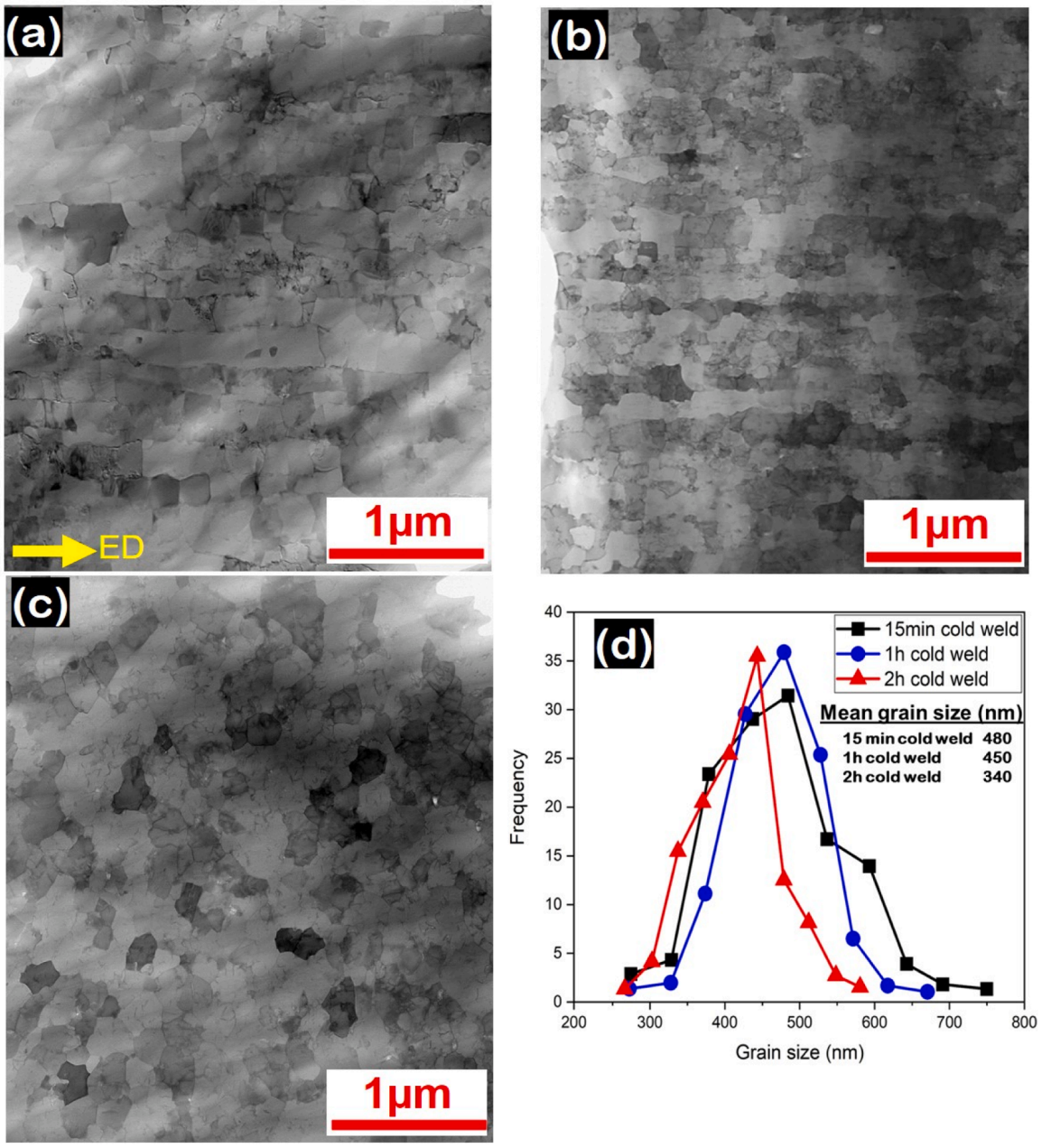

Fig. 6. TEM images of the extruded sample of (a)15 min cold-weld, (b) 1 h cold weld and (c) 2 h cold weld, (d) Grain size distribution and mean grain size of the extruded sample. The yellow arrow showing the extrusion direction (ED).

$$\sigma_y = \sigma_0 + \Delta\sigma_{H-P} + \Delta\sigma_{Al_2O_3} = \sigma_0 + \Delta\sigma_{H-P} + \Delta\sigma^{dis}_{Al_2O_3} + \Delta\sigma^{L-T}_{Al_2O_3} \quad (10)$$

Where σ_0 is a constant of about 10 MPa for Al, based on the Cordero's study [56], σ_{H-P} is the Hall-Petch strengthening of matrix grain refinement, $\Delta\sigma_{Al_2O_3}$ is the strengthening contributions of the native Al_2O_3 nano-dispersoids. As indicated by Eq. (10), the $\Delta\sigma_{Al_2O_3}$ primatily comes from a dislocation strengthening part and a load-transfer strengthening part.

According to the Hall-Petch equation for Al and the matrix grain sizes gained after extrusion, the strengthening contribution from grain refinement, $\Delta\sigma_{H-P}$, is estimated to be about 115 MPa, 130 MPa and 141Mpa for 15 min, 1 h, and 2 h cold weld samples respectively.

A quadratic relationship can be used to calculate the dislocation strengthening:

$$\Delta\sigma_{dis} = \sqrt{(\Delta\sigma_{OR})^2 + (\Delta\sigma^{CTE}_{GND})^2 + (\Delta\sigma^{EM}_{GND})^2} \quad (11)$$

Where $\Delta\sigma_{OR}$ is the contribution of Orowan strengthening, $\Delta\sigma^{CTE}_{GND}$ and $\Delta\sigma^{EM}_{GND}$ account for the geometrically necessary dislocations (GNDs) strengthening arising from the mismatch in coefficient of thermal expansion (CTE) and elastic modulus between reinforcements and matrix. Since the native Al_2O_3 in the composites prepared in this study is platelet shape, modified Orowan-Ashby equation proposed by Nie [57], is used here to calculate the Orowan strengthening of randomly distributed Al_2O_3 as follow:

$$\Delta\sigma_{OR} = \frac{Gb}{2\pi\sqrt{1-\nu}}\left(1.145\sqrt{\frac{0.306\pi dt}{f}} - \frac{\pi d}{8} - 1.061t\right)^{-1} ln\frac{0.981\sqrt{dt}}{b} \quad (12)$$

Where G is the shear modulus of Al at room temperature (26.4Gpa), b is the Burgers vector (0.286 nm, full dislocation of {111}/<110>), ν is the Poisson's ratio (0.33) for pure Al, d, t and f are the mean diameter, mean thickness and volume fraction of the nanoplatelet-like dispersions,